

# STRONG GROUND MOTION IN PORT-AU-PRINCE, HAITI, DURING THE M7.0 12 JANUARY 2010 HAITI EARTHQUAKE

Susan E. Hough and Doug Given  
U.S. Geological Survey  
Pasadena, CA 91106  
USA

Tomoyo Taniguchi  
Dept. of Civil Engineering  
Tottori University  
Tottori, Japan

J-R Altidor, Dieuseul Anglade, and S-L Mildor  
Bureau des Mines et de l'Energie  
Port-au-Prince, Haiti

## ABSTRACT

No strong motion records are available for the 12 January 2010 M7.0 Haiti earthquake. We use aftershock recordings as well as detailed considerations of damage to estimate the severity and distribution of mainshock shaking in Port-au-Prince. Relative to ground motions at a hard-rock reference site, peak accelerations are amplified by a factor of approximately 2 at sites on low-lying deposits in central Port-au-Prince and by a factor of 2.5-3.5 on a steep foothill ridge in the southern Port-au-Prince metropolitan region. The observed amplification along the ridge cannot be explained by sediment-induced amplification, but is consistent with predicted topographic amplification by a steep, narrow ridge. Although damage was largely a consequence of poor construction, the damage pattern inferred from analysis of remote sensing imagery provides evidence for a correspondence between small-scale (0.1-1.0 km) topographic relief and high damage. Mainshock shaking intensity can be estimated crudely from a consideration of macroseismic effects. We further present detailed, quantitative analysis of the marks left on a tile floor by an industrial battery rack displaced during the mainshock, at the location where we observed the highest weak motion amplifications. Results of this analysis indicate that mainshock shaking was significantly higher at this location ( $\sim 0.5g$ , MMI VIII) relative to the shaking in parts of Port-au-Prince that experienced light damage. Our results further illustrate how observations of rigid body horizontal displacement during earthquakes can be used to estimate peak ground accelerations in the absence of instrumental data.

## INTRODUCTION

The 12 January 2010 Mw7.0 Haiti earthquake caused widespread damage in Port-au-Prince as well as smaller cities closer to the mainshock rupture. The extent of damage was primarily due to the proximity of the earthquake to Port-au-Prince, the high vulnerability of many structures, and high population density. Additionally there is the expectation that shaking was amplified by local geologic structure. Port-au-Prince is situated within the Cul de Sac depression, a large rift valley extending north of the city of Port-au-Prince and eastward into the Dominican Republic. Most of the valley is underlain by young and presumably low-impedance Quaternary sediments. The city of Port-au-Prince sits within the southwest corner of the valley; most of this region is underlain by Mio-Pliocene sedimentary deposits, including marl, sandstone, siltstone, and shale, in fans and low foothills. These deposits are expected to be relatively stiff compared to younger and less consolidated Quaternary deposits. However, they are likely to be lower impedance than the adjacent central mountainous core of the southern peninsula. Applying the multi-channel analysis of surface wave (MASW) method, *Cox et al.* (2011) determined Vs30 values at 36 sites throughout Port-au-Prince. Their results indicate that, away from the foothills, Vs30 estimates at sites underlain by Mio-Pliocene deposits are in the range 360-490 m/s, corresponding to NEHRP site class C. Softer sediments, NEHRP class D, are restricted to an  $\sim 0.5$ -2 km wide zone along the coast.

One thus expects that some degree of amplification associated with the relatively low-impedance near-surface materials contributed to the damage within Port-au-Prince. Sediment-induced amplification has been a key factor in the distribution of damage during many recent and historical earthquakes (e.g., *Borcherdt and Gibbs*, 1970; *Singh et al.*, 1985). In general, sediment-induced amplification is controlled by the impedance of near-surface layers and the depth to basement (e.g., *Borcherdt and Gibbs*, 1970; *Su et al.*, 1992; *Joyner*, 2000; *Field*, 2000).

A number of theoretical and observational studies have shown that topographic features, including ridges and cliff faces, can give rise to significant amplification (e.g., *Griffiths and Bollinger*, 1979; *Sanchez-Sesma*, 1985; *Celebi et al.*, 1987; *Hartzell et al.*, 1994; *Spudich et al.*, 1996; *Bouchon et al.* 1996; *Paolucci*, 2002; *Assimaki et al.*, 2005; *Lee et al.*, 2008; *Pishiutta*, 2010). In spite of a growing number of case studies and theoretical studies documenting their significance, topographic effects are generally assumed to be of less importance than sediment-induced amplification. Proxy-based methods for site characterization focus on mapping near-

surface geotechnical properties, usually the average shear-wave velocity in the upper 30 m ( $V_{s30}$ ), that control sediment-induced amplification (e.g., *Wills and Clahan, 2006; Yong et al., 2008; Allen and Wald, 2009*). Methods have not yet been developed to systematically assess and map topographic features that are associated with ground motion amplification.

To investigate the distribution of shaking throughout Port-au-Prince and its relationship to local geological structure, including topography as well as near-surface geology, a total of 9 portable strong-motion instruments were deployed in March-April of 2010 to record aftershocks of the 12 January 2010 earthquake. *Hough et al. (2010)* presented a description of the deployment and preliminary analysis of M3.5-4.5 aftershocks; *Hough et al. (2011)* further explored the hypothesis that the strongest observed amplifications were consistent with expectations for topographic amplification. In this paper we summarize the results presented in earlier studies, and further use detailed and general damage observations to estimate the peak ground accelerations (PGA) in Port-au-Prince during the mainshock.

## OBSERVED AMPLIFICATION

Aftershocks were recorded by nine portable K2 recorders equipped with  $2g$  force-balance accelerometers and, at two stations, velocity transducers (Fig. 1; see *Hough et al., 2010*; data can be accessed via the IRIS Data Management Center). The deployment included a hard-rock reference site (HCEA) in the hills south of Port-au-Prince, where damage during the mainshock was limited in spite of the region's proximity to the rupture; a site on the grounds of the Hotel Montana (HHMT), a site approximately 1 km west of the Hotel Montana (HVCV), and five stations elsewhere in Port-au-Prince. Most of the stations remained in operation through 2010. In this paper we summarize briefly the main findings of *Hough et al. (2010)* and the follow-up investigation of *Hough et al. (2011)* to determine the weak motion amplification estimated from these aftershock records.

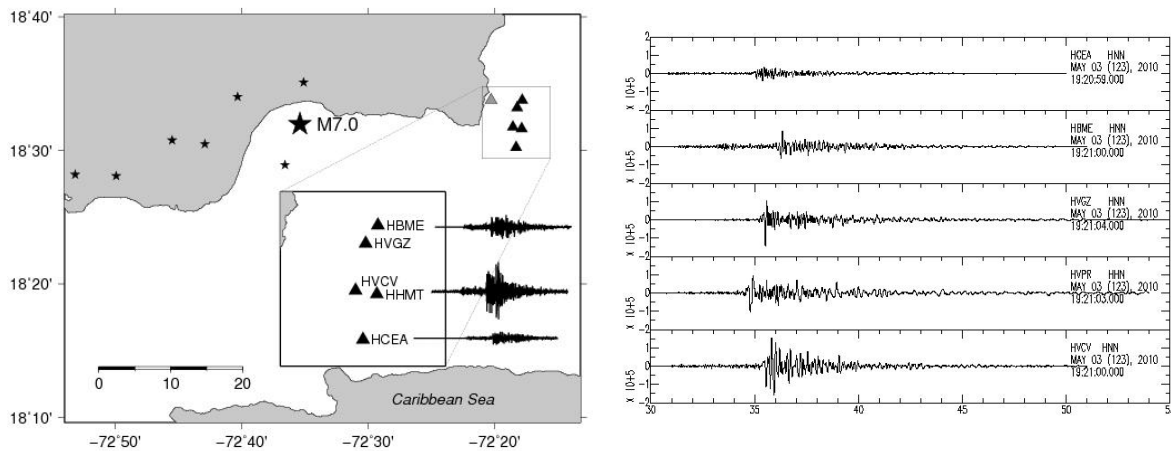


*Fig. 1a. (left) Map showing subset of strong-motion stations (triangles) deployed to record aftershocks (HVPR denoted by gray triangle), an example of waveforms of a moderate aftershock recorded at stations HCEA, HVCV, and HBME, epicenters of some of the aftershocks analysed (small stars) as well as the mainshock (large star). Approximate location of upper edge of mainshock rupture is also shown (dot-dashed line). 1b. (right) NS component of motion for a M4.4 aftershock on 3 May 2010. Record from reference station HCEA is at top; record from HVCV is at bottom. Event is approximately 40 km away from the stations.*

The high-noise urban environment necessitated high (absolute) trigger thresholds. *Hough et al. (2011)* focused on analysis of 11 M3.3-4.5 events recorded between 21 March and 21 September 2010 (e.g., Fig. 1b). These events were recorded by multiple array stations with signal-to-noise levels of a factor of 10 or higher over a frequency range 0.5-30 Hz. These events are all located upwards of 30 km west of Port-au-Prince. The aperture of the array spans a distance of approximately 10 km east-west and north-south, so recordings of the same event at multiple stations will, in general, reflect propagation effects as well as site effects. However, stations HCEA, HHMT, HVCV, HBME, and HVGZ were deployed in a nearly north-south profile across the valley, so the distances from the stations to the aftershocks listed in Table 1 are comparable. *Hough et al. (2011)* focused on analysis of these five stations, which can be used to compute and compare directly amplification at the two stations on the foothill ridge (HVCV, HHMT) with inferred amplification at two stations within the valley, away from the ridge (HBME, HVGZ).

To estimate site response at HBME, HVGZ, HVCV, and HHMT, *Hough et al. (2010)* calculated spectral ratios relative to the reference station using smoothed spectra with a 12-sec window bracketing the S wave (both horizontal components). Spectral ratio from HBME and HVGZ are found to be indistinguishable, so results from these stations are further averaged. *Hough et al. (2010)* showed that ground motions at all valley and foothill stations are systematically amplified relative to ground motions at HCEA. At HHMT the NS component of ground motion is strongly amplified at  $\sim 6$ -8 Hz, with amplification in this band approaching a factor of

5. This amplification is more pronounced on the NS component than the EW component. Ground motions at HVCV are amplified more broadly over 0.5-20 Hz. Ground motions at sites in the valley, at HBME and HVGZ, are also amplified, but less dramatically, between 0.5 and ~10 Hz.

Spectral ratios are in general characterized by high variability, which likely reflects aleatory as well as epistemic uncertainty. One potentially significant source of uncertainty is that ground motions recorded at reference station HCEA are almost certainly influenced to some extent by local site conditions (e.g., *Granswick, 1988*). As discussed by *Hough et al. (2011)*, the average spectral ratios at HHMT and HVCV are only slightly above the mean +1 sigma average spectral ratio from stations HBME and HVGZ. To further explore site response at HHMT and HVCV, *Hough et al. (2011)* considered observed peak ground acceleration (PGA) values. On average, PGA values are amplified relative to HCEA by factors of 1.78 +/- 0.55 (1 sigma) for HBME and HVGZ, versus 2.88 +/- 1.07 for HVCV and HHMT. Considering the stations separately, PGA amplification is 3.57 +/- 0.79 at HVCV, 2.31 +/- 0.85 at HHMT, 1.75 +/- 0.36 at HBME, and 1.82 +/- 0.71 at HVGZ (Fig. 2). Estimated PGA amplification is 2.1 +/- 0.64 for station HVPR. This site is within about 1 km of the coast, and the main port, in an area presumably underlain by soft sediments. The station recorded relatively few events due to a high trigger threshold necessitated by high noise conditions. It is also several kilometers west of the other stations considered. Nonetheless, the estimated PGA amplification, while not well constrained, is only slightly higher than that at HBME and HVGZ. Further work will be needed to assess amplification at NEHRP Class D/E sites in Port-au-Prince.

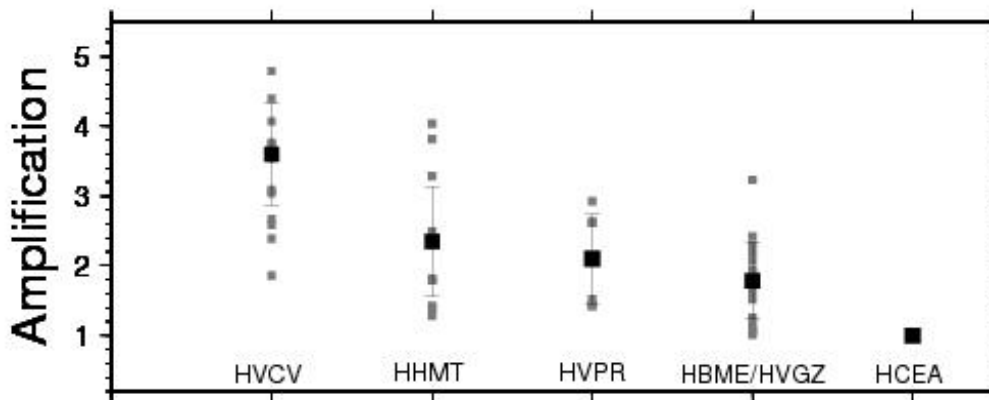
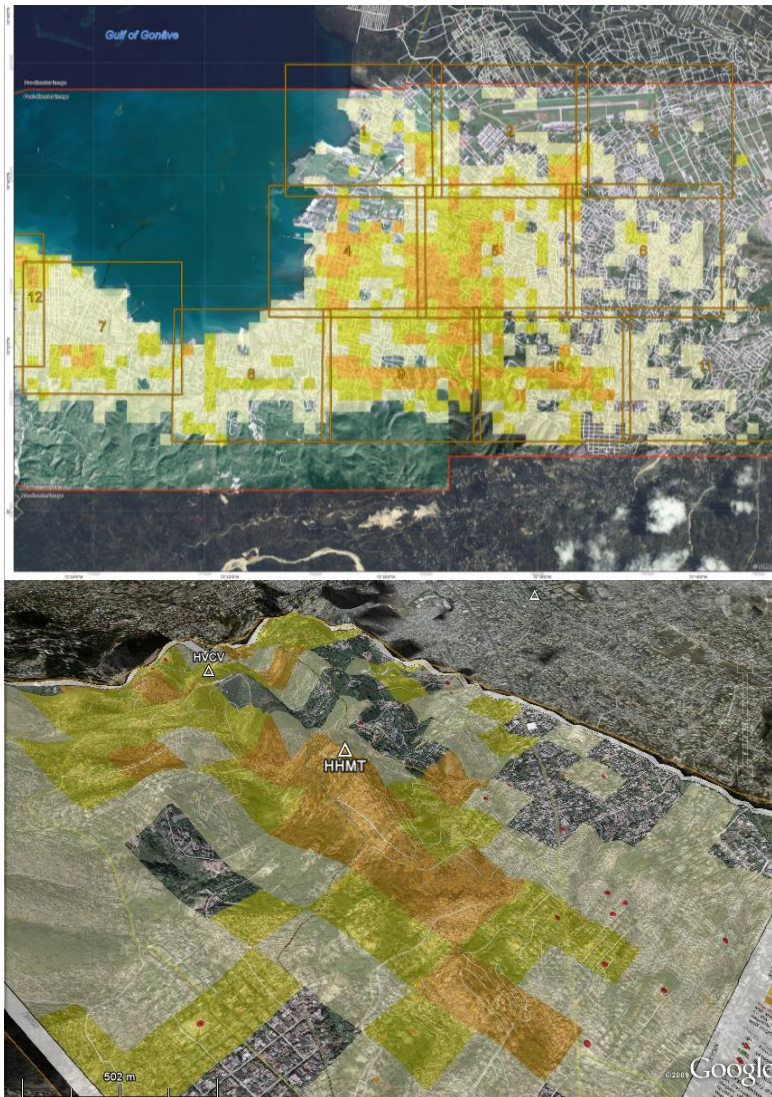


Fig. 2. Estimated weak-motion PGA amplification factors at stations indicate, for individual events (small gray squares) and averages (+/- 1  $\sigma$ ) at each station. Amplifications calculated relative to reference station HCEA.

Surveying the K2 and other sites using a shallow surface wave technique (MASW), *Cox et al. (2011)* showed that the foothill stations are, as expected, characterized by higher Vs30 values than stations in the adjacent valley: 505 m/s and 626 m/s at HVCV and HHMT, respectively, compared to 427 m/s and 451 m/s at HBME and HVGZ, respectively. (*Cox et al. (2011)* estimated values of 303 m/s at HVPR, and 1014 m/s at HCEA). The estimated high PGA amplifications at HHMT and HVCV thus cannot be explained by traditional sediment-induced amplification. *Hough et al. (2011)* showed that the observed amplitude, predominant periods, variability, and polarization of amplification are consistent with predicted topographic amplification by a steep, narrow ridge.

## DAMAGE DISTRIBUTION

Due to the paucity of ground motion recordings for Port-au-Prince, weak-motion amplification factors cannot be estimated for other sites. One can, however, consider the distribution of damage to further explore the association between topography and shaking intensity. The city of Port-au-Prince sustained substantial damage during the 2010 earthquake. Serious damage occurred throughout the greater metropolitan area (Figure 3a), but the level of damage varied considerably, with pockets of greater and lesser damage throughout the city. Haiti's Ministry of Public Works, Transport, and Communications (MTPTC) implemented an extensive damage assessment program, including training teams of local engineers who evaluated 400,000 structures throughout Port-au-Prince (Kit Miyamoto, pers. comm., 2010). Approximately 50% of the structures were assessed as having no serious structural damage; 30% were observed to have significant but reparable damage; 20% suffered collapse or irreparable damage. The full results of this assessment are not currently available. However, the increasing availability of high-quality satellite data now allows for rapid damage assessments to be made from remote-sensing imagery. For example, in the immediate aftermath of the earthquake, scientists at the German Aerospace Center (DLR) collected, processed, and analyzed radar and optical data to develop a damage map for the city ([http://www.dlr.de/en/desktopdefault.aspx/tabid-6213/10205\\_read-220](http://www.dlr.de/en/desktopdefault.aspx/tabid-6213/10205_read-220)). The DLR map assesses damage within grid cells 250-m square according to the percentage of damaged buildings: <10%, 10-40%, and >40% (Fig. 3). Focusing on the sheet that covers the foothill ridge (Fig. 3b), the variability of damage is evident.



*Fig. 3a. (top) Damage distribution for the 12 January 2010 mainshock determined by the DLR (see text) from analysis of remote-sensing imagery. Colors indicate estimated percent building damage: 0-10% (tan), 10-40% (yellow), >40% (orange). 3b. (bottom) Damage in the southern metropolitan Port-au-Prince region draped over topography (x3 vertical exaggeration). Stations HVCV and HHMT (white triangles) are located along a narrow, roughly east-west trending ridge. View towards the northwest.*

In the southern metropolitan Port-au-Prince region (Fig. 3b), damage was generally less severe than in the rest of the city. This part of the city is generally more affluent, so structures are generally of better quality: Masonry C or in some cases B (well-built masonry, not specifically designed to reduce lateral forces), whereas poor-quality masonry (Masonry D) is prevalent throughout much of the rest of the city. However, there has been an absence of effective, enforced land-use planning in Haiti; shanty towns characterized by extremely poor construction have developed throughout the city, including within the relatively affluent southern foothills. The distribution of damage, even in this region, is thus expected to reflect a number of different factors beyond ground motion severity.

Notwithstanding the expectation that the damage distribution is a coarse and imprecise indication of the shaking distribution, the draped damage distribution (Fig. 3b) suggests a correspondence between the band of high damage and the narrow foothill ridge. Topographic profiles cutting across the ridge at the locations of HHMT and HVCV (Fig. 4) further illustrate this correspondence. At HVCV, the band of high damage extends over a pair of sub-parallel ridges. At HHMT damage is low in the hills above the ridge, increasing significantly at the base of the ridge. Damage appears to drop to the north of HHMT, but there were few structures on the steep hillside immediately north of the hotel. The hotel complex itself included two multi-storey structures built against the hillside; one building survived the earthquake, the other collapsed catastrophically. Mainshock ground motions and damage at HVCV will be discussed in the following section. The third panel in Fig. 4 is along a road running northward away from the airport, which can be seen in the upper-right-hand corner of Fig. 3a. Damage in this part of Port-au-Prince, which is relatively distant from the mainshock,

was generally lighter than in the more central parts of the metropolitan region. However, as shown in Fig. 4, a small pocket of heavy damage coincides with an especially steep hill.

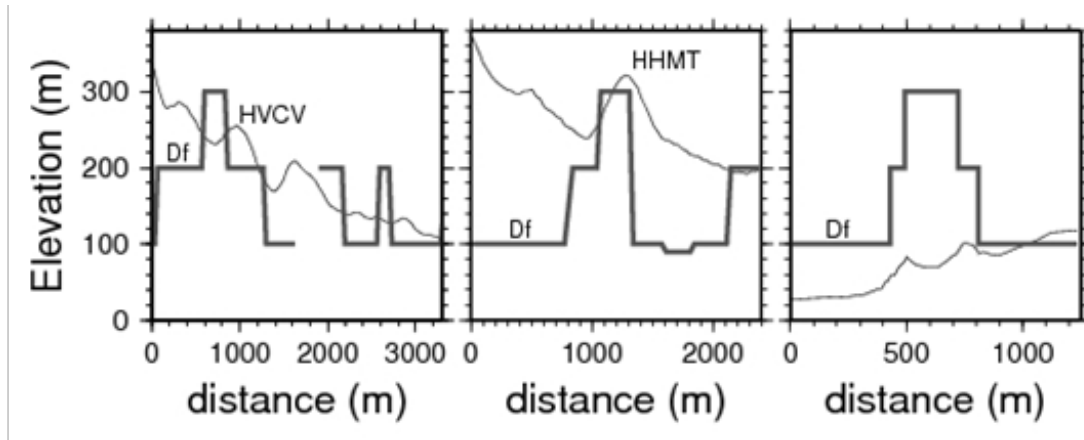


Fig 4. Topographic profiles running southwest-northeast through station HVCV (left), and HHMT (center). Also shown is a profile running north-south from the airport (right). Scaled damage factor,  $D_f$ , shown on each panel (heavy gray lines: arbitrarily set values corresponding to 300, 200, and 100 m correspond to orange, yellow, and tan in Figure 2)

#### MAINSHOCK GROUND MOTIONS

Both aftershock recordings and the damage distribution suggest that shaking severity was significantly amplified by small-scale topographic features, including small hills and ridges. The question remains, how strong was the mainshock shaking in Port-au-Prince? In the absence of instrumental recordings of mainshock ground motions, well-constrained intensity values have been shown to provide surprisingly reliable estimates of peak ground acceleration and velocity (e.g., *Atkinson and Wald, 2007*). A thorough, systematic assessment of seismic intensities, properly taking structural vulnerability into account, has not been done to-date. However, a handful of well documented direct eyewitness accounts suggest relatively moderate shaking severity. For example, a direct eyewitness survey revealed that, in the well-built commercial structure shown in Fig. 5a, shaking severity was only Modified Mercalli Intensity (MMI) V: a few small objects overturned, no cracks or structural damage, pictures hung on nails knocked askew but not off of the walls, etc. The buildings on both sides of this structure collapsed catastrophically. Similarly, the house shown in Fig. 5b, which can reasonably be assumed to be of ordinary masonry construction and ordinary workmanship, neither reinforced nor designed to resist lateral forces, sustained only very minor, surficial cracks, and some toppling of small objects, indicating MMI VI. Many nearby structures, including a school building directly adjacent to the house, sustained catastrophic damage or collapse, presumably as a result of extreme vulnerability.

Macroseismic intensities for the Haiti earthquake were also determined from a total of almost 1000 reports submitted to the Community Internet Intensity Map (“Did You Feel It?”) site (*Wald et al., 1999*). A total of 16 accounts were submitted from Port-au-Prince as of June 2011, from which an average numerical intensity of 7.4 was determined. It is not known where within the city the accounts were from; the examples described above as well as the damage distribution indicate that areas with low damage (0-10% building damage) experienced mainshock intensities less than 7.4. We conclude that MMI V-VI is a reasonable assignment for the parts of the city that sustained light damage. *Wald et al. (1999)* infer PGA ranges of 3.9-9.2 %g for MMI V and 9.2-18 %g for MMI VI for earthquakes in California. *McNamara et al. (2011)* show that  $S$  and  $Lg$ -wave attenuation in Hispaniola is comparable to attenuation in California. We thus conclude that PGA values in the range 10-15 %g are reasonable estimates for shaking severity in parts of Port-au-Prince where damage was light.

The above considerations, as well as the lack of substantial damage to over half of the houses in Port-au-Prince despite pervasively poor construction, suggest that parts of Port-au-Prince did not experience severe mainshock ground motions. This conclusion is supported by ground motion prediction equations established for other tectonically active, and presumably analogous, regions; they predict an average PGA on stiff-soil (NEHRP Class C) sites of approximately 0.15g for a M7.0 earthquake at 20-km distance (e.g., *Campbell and Bozorgnia, 2006*). We note that predicted PGA values from established prediction equations provide only a rough estimate of shaking. In this case, among other issues, it is not clear what distance is appropriate, since the majority of the mainshock moment release was to the west of the epicenter. However, this consideration yields an estimate that is consistent with the estimate based on damage. Taking 0.10-0.15g as a range for PGA in the low-damage (0-10% building damage) regions, PGA in regions of greater damage can be estimated from weak-motion amplification factors determined from aftershock recordings.



Figure 5a (left) A good-quality commercial structure in which MMI V-VI is estimated based on an eyewitness interview; 5b (right) a private home, masonry C construction, for which MMI VI is estimated. The structures on both sides of the structure shown in 5a collapsed catastrophically, as did a school building adjacent to the house shown in 5b.

As described earlier, analysis of aftershocks recorded across the array reveals weak motion PGA amplification of  $3.6 \pm 0.8$  at station HVCV, with suggested resonance peaks at 2-3 Hz and 5-6 Hz (Hough *et al.*, 2010; Hough *et al.*, 2011). Assuming linearity of response and a mainshock PGA of 0.10-0.15g in the absence of local amplification, these results imply mainshock PGA of roughly 0.28-0.66g at HVCV. We note that this range of PGA values is consistent with the range estimated independently by Goodno *et al.*, (2011). Their study used a similar approach, inferring PGA values from damage observations, so consistency between the studies is not surprising. However, Goodno *et al.* [2011] consider detailed independent observations of damage to structures and electrical systems at key sites in Port-au-Prince and compare the results with both general PGA-damage associations and associations developed from observations following the 1971 Sylmar, California earthquake.

#### Analysis of “Batterygram” at HVCV

An apparently well built, engineered two-story building at the other station, HVCV, sustained little structural damage (Figure 6a). On the grounds of the cell phone facility a retaining wall and part of the parking lot collapsed (Fig. 6b) and cinderblock walls fell. Some damage was sustained to the upper corner of the building, but had been repaired by the time our field team first visited the site in March 2010. Interviews with employees who were in the building at the time reveal that shaking within the building was strong enough to topple computer monitors, free-standing counters and other furniture, and to knock people to their feet several times when they tried to run. In the residential neighborhood to the immediate west of HVCV almost all houses collapsed catastrophically. All of these structures, however, were unreinforced masonry of extremely poor construction. Within approximately 1/2 kilometer of HVCV a recently completed, apparently well-built commercial structure sustained substantial damage (Fig. 7); this structure was not salvageable, and by November 2010 it had been demolished.



Figure 6a. (left) Canape Vert Voila cell phone facility; 6b. (right) collapse of retaining wall in parking lot. The face of the building seen in the photograph is aligned roughly N-S; the battery racks discussed in this study are located on the ground floor, in a large room behind the doors seen at left in Fig. 6a.



*Figure 7. Damage to recently built commercial building approximately 0.5 kilometer west of HVCV. The building was later demolished.*

At HVCV shaking was strong enough to displace heavy industrial battery racks on the ground floor of the Voila building shown in Fig. 6a. The battery rack shown in Fig. 8 was one of several rows of similar racks in a large room on the ground floor of the northwest side of the building. Several individual racks had been moved by the earthquake; the one shown in Figure 8 experienced the largest displacement and left the clearest and most accessible marks on the floor. This rack holds a total of 24 batteries: six rows of four. Each battery weighs approximately 320 lbs; the weight of the batteries is thus approximately 7680 lbs. The weight of the rack itself is unknown but is estimated to be a small percentage of the battery weight. The rack is 141 cm long, 172 cm tall, and 56 cm wide including the full width of the feet, approximately 40 cm without the feet. The height/width aspect ratio is thus approximately 4:1.



*Fig. 8a. (left) Rack of batteries that was moved across the floor during the mainshock. The near (short) edge of the front rack is aligned roughly N-S, with the closest edge towards the south. 8b (right) close-up of scratches left on tile, including pen marks drawn to indicate inferred trajectory. (The loop is inferred to have been left by a remnant of the bolt that was dragged as the rack moved)*

The close-up photograph of the floor near the rack (Fig. 8b) reveals two holes where two adjacent racks were anchored. The southernmost rack (to right in Fig. 8a) was initially set into motion towards the south; the neighboring rack moved towards the north. We suggest the most likely explanation for the opposite directions of motion is that the racks collided with each other as a result of initial shaking, and bolts holding down both racks were broken at least in part as a consequence of the force of the reaction. Once the racks were free to move, the northern rack may have interacted with the neighboring rack on the other side (towards back of Fig. 8a), but the southern rack moved only in response to earthquake ground motions. According to this interpretation, the initial southward displacement of the rack, approximately 30 cm, resulted from a combination of collisional forces and the force associated with ground acceleration. During this excursion towards the south the rack also moved approximately 24 cm to the west. This westward component of motion cannot have been a consequence of the collision, which acted in a nearly perpendicular direction. The two subsequent displacements, approximately 22 cm and 27 cm, respectively, are also inferred to be a consequence of ground acceleration.

Once the bolts were broken, the coefficient of friction was significantly reduced, allowing the rack to slide. The scratch marks on the floor reveal no evidence for subsequent rocking after the bolts were broken. The coefficient of friction during sliding is unknown, but we can estimate an upper bound given that the rack did not rock after the bolts were broken. We can then explore the range of PGA and predominant period of motion that will generate a displacement of 22-27 cm.

The coefficient of friction between the steel legs of the rack and the floor is a key parameter for our analysis, and is unknown. Established values for the coefficient of friction between steel and other materials are almost universally higher than 0.2, except for extremely slippery materials such as graphite and Teflon. The ceramic tile floor is relatively slippery, but presumably less slippery than Teflon. We therefore consider  $\mu = 0.15-0.20$  to be a reasonable estimate, and consider values of 0.15 and 0.20 in our calculations.

The displacement of a rigid body subjected to horizontal accelerations resulting from an earthquake was first investigated by *Housner* (1963). In this study we use the results of *Taniguchi and Miwa* (2007), who approximated the slip displacement of a rectangular rigid body in an earthquake with the displacement resulting from sinusoidal base accelerations. (We will discuss the additional complication of vertical acceleration in a following section.) *Taniguchi and Miwa* (2007) showed that, in response to horizontal sinusoidal motion, the maximum relative displacement of a rigid body is given by

$$x_{sin} = 1/2\mu gt_1^2 + (A_{gx}gTp^2/4\pi^2)\sin(2\pi t_1/T) + D_1 t_1 + D_2 \quad (1)$$

where

$$D_1 = -\mu gt_0 - (A_{gx}gTp/2\pi)\cos(2\pi t_0/Tp) \quad (2)$$

$$D_2 = 1/2(\mu gt_0^2) - (A_{gx}gTp^2/4\pi^2)\sin(2\pi t_0/Tp) + (A_{gx}gTpt_0/2\pi)\cos(2\pi t_0/Tp) \quad (3)$$

and  $t_0$  and  $t_1$  are the beginning and end times of motion given by,

$$t_0 = (Tp/2\pi)\sin^{-1}(\mu/A_{gx}) \quad (4)$$

$$t_1 = Tp/(2pA_{gx})[(\mu - \pi t_0 A_{gx}) + \sqrt{((\mu - \pi t_0 A_{gx})^2 + 2A_{gx}(\psi + A_{gx}(1 - \pi^2/2)))}] \quad (5)$$

where

$$\psi = \mu \sin^{-1}(\mu/A_{gx}) + A_{gx} \cos(\sin^{-1}(\mu/A_{gx})) \quad (6)$$

$A_{gx}$  and  $Tp$  are the peak acceleration ( $PGA = A_{gx}g$ ) and predominant period of acceleration, respectively. We use equation (1) to calculate  $x_{sin}$  for  $A_{gx} = 0.1 - 1.5g$  and  $T = 0.5 - 1$  s, assuming  $\mu$  values of 0.15 and 0.20.

A further consideration is that, as discussed by *Taniguchi and Miwa* (2004), predicted slip from input sinusoidal motions,  $x_{sin}$ , will differ from predicted slip from earthquake ground motions. On average, the mean ratio between exact displacement and  $x_{sin}$  is approximately 1. That is, 50% of earthquakes with a given  $A_{gx}$  are expected to produce a horizontal displacement greater than  $x_{sin}$ . Considering 104 earthquake records from sites around Japan, *Taniguchi and Miwa* (2004) determine the probability density function (pdf) for a slip ratio,  $\beta_{prob}$ :

$$x_{exp} = \beta_{prob} \cdot x_{sin} \quad (7)$$

Using the 104 recordings, *Taniguchi and Miwa* (2004) derive values of  $\beta_{prob}$  of 1.84 and 2.32 corresponding to probabilities of nonexceedance of 90% and 95%, respectively. Thus, to obtain a more statistically rigorous estimate of acceleration due to earthquake shaking,  $A_{gx}^{eq}$ , we should consider a target displacement of (22-25 cm)/1.84 to obtain an estimate of  $A_{gx}^{eq}$  with a 90% probability of nonexceedance, or (22-25)/2.32 for a 95% probability of nonexceedance. In the following section we will use a target displacement of 12-15 cm to estimate  $A_{gx}^{eq}$  with a 90% probability of nonexceedance.

The results shown in Fig. 9 reveal that the range of  $A_{gx}/Tp$  values that predict a displacement of 12-15 cm do not differ significantly for the assumed values of  $\mu$ . In both cases,  $A_{gx}$  is upwards of  $0.7g$  for  $Tp=0.5s$ , a value that is consistent with the lowest site response peak inferred from weak motion recordings. Given the proximity of the mainshock to the site it is likely that mainshock ground motions were controlled by longer period energy. We consider the range 0.5 – 1 s to be a reasonable range for  $Tp$ . This range corresponds to  $A_{gx}$  values of roughly 0.33-0.72g for the values of  $\mu$  considered.

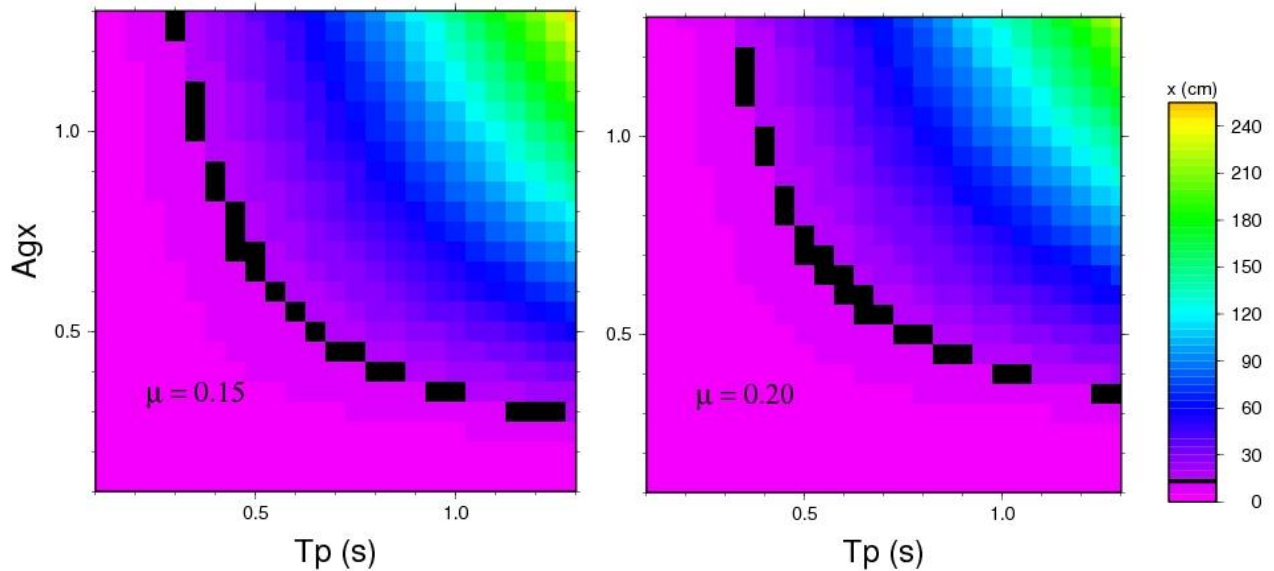


Fig. 9. Predicted displacement in cm (color scale indicated) as a function of predominant period of shaking,  $T_p$ , and peak acceleration ( $A_{gx}g$ ) for  $\mu$  values of 0.15 (left), 0.20 (right). Black swath indicates values that predict maximum displacement values of 12-15 cm, the target displacement to estimate  $A_{gx}^{eq}$  with a 90% probability of nonexceedance.

A final consideration is that the combination of gravity and vertical ground acceleration may increase or decrease the slip displacement. At this site, aftershock recordings reveal that the horizontal components of motion are systematically (and typically) amplified relative to the vertical component by a factor of approximately 2 over a frequency range 0.4-10 Hz (Figure 10b). As noted by *Taniguchi and Miwa* (2007), the effects of varying vertical acceleration of the body will have minimal contribution to the displacement given the short time a body is in motion. To provide an adequate safety margin for predictions of displacement for a given ground motion, *Taniguchi and Miwa* (2007) assume a monotonous reduction in friction due to vertical acceleration. For a body on a ground floor, the nominal coefficient of friction,  $\mu'$ , is given by

$$\mu' = \mu(1 - PVGA(\sigma/g)) \quad (7)$$

where PVGA is the peak vertical ground acceleration and  $\sigma$  is the standard deviation of the ratio of the vertical ground acceleration to the peak vertical ground acceleration at the instant of the peak horizontal shaking. In this study we are not seeking to predict displacement for a given ground motion but rather to infer ground motion for a given displacement. The effects of varying vertical acceleration, which could either increase or decrease effective friction, are unknowable but will introduce an additional factor of uncertainty.

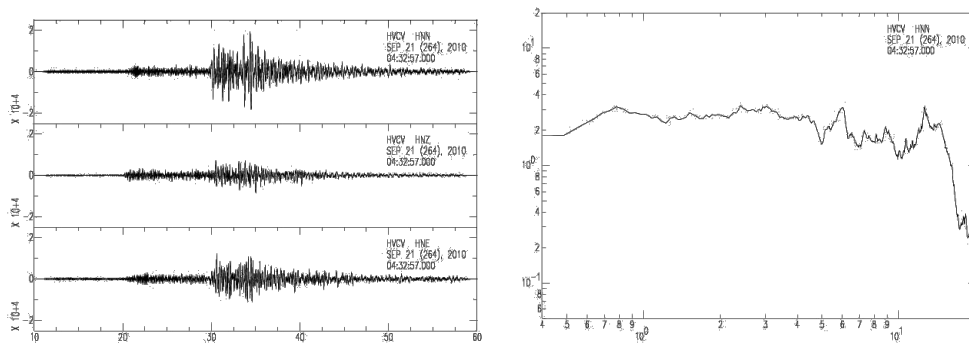


Figure 10a (left). Three components of ground motion (NS top, V middle, EW bottom) for a M4.4 aftershock recorded at HVCV. 10b (right) NS/V spectral ratio.

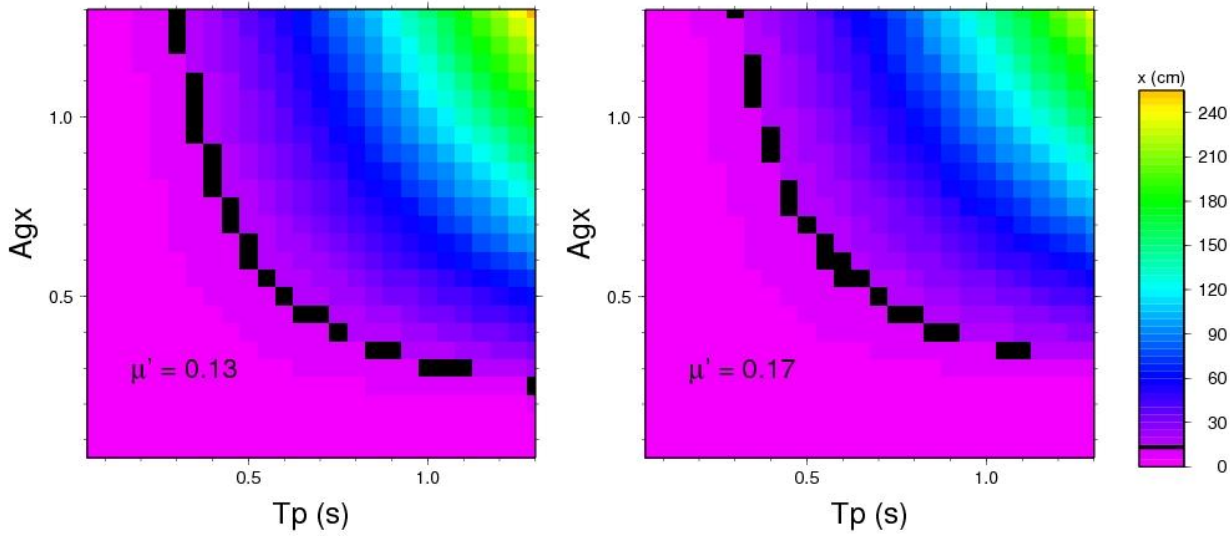


Fig. 11. Predicted displacement in cm (color scale indicated) as a function of predominant period of shaking,  $T_p$ , and peak acceleration ( $A_{gx}g$ ) for  $\mu'$  values of 0.13 (left), 0.17 (right). Black swath indicates values that predict maximum displacement values of 12-15 cm, the target displacement to estimate  $A_{gx}^{eq}$  with a 90% probability of nonexceedance.

To explore the possible effect of vertical accelerations we assume  $\sigma = 0.46$  and vertical acceleration, PGVA, to be 0.5 horizontal PGA, following Taniguchi and Miwa (2007). Assuming horizontal PGA of 0.6g and that vertical acceleration monotonically lowers  $\mu'$ , equation (3) yields  $\mu' = 0.86\mu$ . If we lower our estimates of  $\mu$  from 0.15 and 0.20 accordingly (i.e., to 0.13 and 0.17), the range of inferred  $A_{gx}$  values is lowered only slightly (Fig. 11). For example, for  $T_p = 0.5$  s, the  $A_{gx}$  value that predicts a displacement of 15 cm is 0.65g for  $\mu' = 0.13$  versus 0.70 for  $\mu' = 0.15$ . As discussed by Taniguchi and Miwa (2007), the target displacement also changes if one considers the effects of vertical base acceleration. For 90% probability of exceedance, the target displacement is 13.0 -14.8 cm (i.e., (22-25 cm)/1.69) rather than 12.0 - 13.6 (i.e., (22 - 25)/1.84). Given the limitations in precision of the estimated displacements, this difference is not consequential.

## DISCUSSION AND CONCLUSIONS

We have used carefully considered macroseismic observations, ground motion prediction equations, and forensic analysis of a case of rigid body displacement to estimate the severity of ground motions in Port-au-Prince during the 12 January 2010 Haiti earthquake. Each step of the analysis is characterized by significant uncertainties. However, we are able to determine two independent estimates of mainshock PGA at HVCV: 0.28-0.66g based on an assessment of macroseismic intensity in the lightly damaged parts of Port-au-Prince combined with the estimated weak-motion amplification at HVCV, and 0.33-0.72g based on independent analysis of the “batterygram.” Analyzing the batterygram, a key unknown is the predominant period of acceleration; the results are relatively insensitive to values of  $\mu$  varied within reasonable bounds. The consistency of these estimates, which are entirely independent, is encouraging. We thus conclude that mainshock PGA at HVCV was approximately 0.5g, which corresponds to MMI VIII. Our overall results suggest that local amplifications, in some cases associated with topographic effects, increased shaking intensity by approximately two units, from MMI VI to VIII. The inevitable future rupture of the Enriquillo Plantain Garden fault segment closest to Port-au-Prince is expected to generate generally higher near-field ground motions within the city than those generated by the 2010 earthquake. Ground motions from such an event are expected to be especially severe at sites with strong local amplification.

The results presented in this study also suggest that forensic analysis of rigid body displacement during earthquakes can provide reliable, quantitative estimates of shaking intensity, using the theoretical formulation developed by Taniguchi and Miwa [2004] and Taniguchi and Miwa [2007]. Further application of this approach might help constrain mainshock ground motions at other locations in Port-au-Prince, for example at the sites where damage was documented by Goodno *et al.* [2011].

## ACKNOWLEDGMENTS

We are indebted to the individuals who provided support for the instrument deployment: Gerard Laborde and Gregory Domond from Voila corporation; the owners of the Hotel Montana; the US Army Corps of Engineers; the staff of the Plaza Hotel; Jean-Henry and Chantal Ceant; Gregory Groth, David Lindwall, and other personnel at the US Embassy in Port-au-Prince. We thank Brady Cox for

making his Vs30 values available, and acknowledge Elizabeth Cochran and Bob Dollar for constructive reviews that improved the manuscript. Work was supported by USAID-Office of Foreign Disaster Assistance.

## REFERENCES

- Aki, K [1993]. Local site effects on weak and strong ground motion, *Tectonophysics*, 218, pp. 93-111.
- Allen, T.I. and D.J. Wald [2009]. On the use of high-resolution topographic data as a proxy for seismic site conditions (Vs30), *Bull. Seism. Soc. Am.* 99, pp. 935-943.
- Assimaki, D., *et al.* [2005]. Effects of local soil conditions and topographic aggravation of seismic motion: Parametric investigation and recorded field evidence from the 1999 Athens earthquake, *Bull. Seism. Soc. Am.* 95, pp. 1059-1089.
- Atkinson, G. and D. Wald [2007]. Modified Mercalli Intensity: A surprisingly good measure of ground motion, *Seism. Res. Lett.* 78, 363- 368.
- Borcherdt, R.D. and J.F. Gibbs [1970]. Effects of local geology on ground motion near San Francisco Bay, *Bull. Seism. Soc. Am.*, 60, 29-61.
- Bouchon, M., et al. [1996]. Effect of three-dimensional topography on seismic motion, *J. Geophys. Res.* 101, pp. 5835-5846.
- Campbell, K. and Bozorgnia [2008]. NGA ground motion model for the geometric mean horizontal component of PGA, PGV, PGD, and 5% damped linear elastic response spectra for periods ranging from 0.01 to 10 s, *Earthq. Spectra*, 24, pp. 139-171.
- Celebi, M. [1987]. Topographical and geological amplifications determined from strong-motion and aftershock records of the 2 March 1985 Chile earthquake, *Bull. Seism. Soc. Am.*, 77, pp. 1147-1167.
- Calais, E. et al. [2010] Strain partitioning and fault slip rates in the northern Caribbean from GPS measurements, *Geophys. Res. Lett.* 29, doi: 10.1029/2002GL015397.
- Calais, E., et al. [2010] Transpressional rupture of an unmapped fault during the 2010 Haiti earthquake, *Nature Geoscience* 3, 794-799, doi:10.1038/NGEO992.
- Cox, B.R., et al. [2011]. Shear-wave-velocity and geology-based seismic microzonation of Port-au-Prince, Haiti, in press, *Earthq. Spectra*.
- Field, E.H. [2000]. A modified ground-motion relationship for southern California that accounts for detailed site classification and a basin-depth effect, *Bull. Seism. Soc. Am.* 90, pp. S209-S221.
- Goodno, B.J., et al. [2011]. Effects of the January 2010 Haitian earthquake on selected electrical equipment, in press, *Earthq. Spectra* (2011).
- Griffiths, D.W. and G.A. Bollinger [1979]. Effect of Appalachian mountain topography on seismic waves, *Bull. Seism. Soc. Am.* 69, pp. 1081-1105.
- Hartzell, S.H., et al. [1994]. Initial investigation of site and topographic effects at Robinwood Ridge, California, *Bull. Seism. Soc. Am.* 84, 1336-1349.
- Housner, G.W. [1963]. The behavior of inverted pendulum structures during earthquakes, *Bull. Seism. Soc. Am.* 53, 403-417.
- Hayes, G.P, et al., [2010]. Complex rupture during the 12 January 2010 Haiti earthquake, *Nature Geoscience* 3, 800-805, doi:10.1038/NGEO977.
- Hough, S.E., et al. [2010]. Localized damage associated with topographic amplification during the 12 January 2010 M7.0 Haiti earthquake, *Nature Geoscience* 3, 778-782.
- Hough, S.E., et al. [2011]. Site response and site characterization in Port-au-Prince, Haiti, in press, *Earthq. Spectra*.

- Joyner, W.B. [2000]. Strong motion from surface waves in deep sedimentary basins, *Bull. Seism. Soc. Am.* 90, pp S95-S112.
- Lee, S.J., et al. [2009]. Effects of realistic surface topography on seismic ground motion in the Yangminshan region of Taiwan based on the spectral-element method and LiDAR DTM, *Bull. Seism. Soc. Am.* 99, 681-693.
- Mann, P., et al. [1992], An overview of the geologic and tectonic development of Hispaniola, *Geol. Soc. Am. Special Paper* 262, pp. 1-28.
- McNamara, D. et al. [2011], Frequency dependent attenuation of the Hispaniola Island and surrounding regions, in review, *Bull. Seism. Soc. Am.*
- Paolucci, R. [2002]. Amplification of earthquake ground motion by steep topographic irregularities, *Earthq. Eng. And Struct. Dyn.*, 31, pp 1831-1853.
- Pischiutta, M., G. [2010]. effects on the hill of Nocera Umbria, central Italy, *Geophys. J. Int.* 182, pp. 977-987.
- Sanchez-Sesma, F. J. [1985]. Diffraction of elastic SH waves by wedges, *Bull. Seism. Soc. Am.* 75, pp. 1435-1446.
- Shenton, H.W. and N.P. Jones [1992]. Effect of friction and restitution on rocking motions, *Earthq. Eng.*, Tenth World Conference, 1933-1938.
- Singh, S.K. et al. [1988]. Some aspects of source characteristics of the 19 September 1985 Michoacan earthquake and ground motion amplification in and near Mexico City from strong motion data, *Bull. Seism. Soc. Am.* 78, pp. 451-477
- Spudich, P. et al. [1996]. Directional topographic site response at Tarzana observed in aftershocks of the 1994 Northridge, California earthquake: Implications for mainshock motions, *Bull. Seism. Soc. Am.* 86, pp. S193-S208.
- Taniguchi, T. [2002]. Non-linear response analyses of rectangular rigid bodies subjected to horizontal and vertical ground motion, *Earthq. Eng. and Structural Dyn.*, 31, pp. 1481-1500, doi: 10.1002/eqe/170.
- Taniguchi, T. and T. Miwa [2004]. Slip displacement analysis of freestanding rigid bodies subjected to earthquake motions, proceedings, 13<sup>th</sup> World Conference on Earthquake Engineering, Vancouver, Paper 437.
- Taniguchi, T. and T. Miwa [2007]. A simple procedure to approximate slip displacement of freestanding rigid body subjected to earthquake motions, *Earthq. Eng. and Structural Dyn.*, 36, 481-501 doi: 10.1002/eqe.639.
- Wald, D.J., et al. [1999]. Relationships between peak ground acceleration, peak ground velocity, and modified Mercalli intensity in California, *Earthq. Spectra* 15, 557-564.
- Wills, C.J. et al. [2000]. A site-conditions map for California based on geology and shear-wave velocity, *Bull. Seism. Soc. Am.* 90, pp. S187-S208.
- Yong, A. et al. [2008]. Quantification of site characterization from remote-sensing data, *Bull. Seism. Soc. Am.* 98, pp. 2679-2693.